






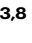


Efficient generation of human NOTCH ligand-expressing haemogenic endothelial cells as infrastructure for in vitro haematopoiesis and lymphopoiesis

Received: 26 February 2023

Accepted: 14 August 2024

Published online: 04 September 2024

 Check for updates

Shicheng Sun ^{1,2,3,6,7} , Ali Motazedian^{1,4,5,7}, Jacky Y. Li^{1,2,3}, Kevin Wijanarko^{1,2,3}, Joe Jiang Zhu ^{4,5}, Kothila Tharmarajah^{1,2,3}, Kathleen A. Strumila^{1,2,3}, Anton Shkaruta^{1,2,3}, L. Rayburn Nigos^{1,3}, Jacqueline V. Schiesser^{1,2,3}, Yi Yu^{1,2}, Paul J. Neeson ^{4,5}, Elizabeth S. Ng ^{1,2,3}, Andrew G. Elefanty ^{1,2,3,8} & Edouard G. Stanley ^{1,2,3,8} 

Arterial endothelial cells (AECs) are the founder cells for intraembryonic haematopoiesis. Here, we report a method for the efficient generation of human haemogenic DLL4⁺ AECs from pluripotent stem cells (PSC). Time-series single-cell RNA-sequencing reveals the dynamic evolution of haematopoiesis and lymphopoiesis, generating cell types with counterparts present in early human embryos, including stages marked by the pre-haematopoietic stem cell genes *MECOM/EVIL*, *MLLT3* and *SPINK2*. DLL4⁺ AECs robustly support lymphoid differentiation, without the requirement for exogenous NOTCH ligands. Using this system, we find IL7 acts as a morphogenic factor determining the fate choice between the T and innate lymphoid lineages and also plays a role in regulating the relative expression level of *RAG1*. Moreover, we document a developmental pathway by which human *RAG1*⁺ lymphoid precursors give rise to the natural killer cell lineage. Our study describes an efficient method for producing lymphoid progenitors, providing insights into their endothelial and haematopoietic ontogeny, and establishing a platform to investigate the development of the human blood system.

The study of human haematopoietic development underpins our understanding of congenital immune disorders and provides guidelines for the in vitro production of immune cells for applications in discovery research and cell therapies. Mouse studies have contributed significantly to our understanding of embryonic haematopoiesis^{1–9}, including its location, endothelial origin, and the factors affecting cell

fate determination of immune cell lineages. Nevertheless, there is increasing evidence pointing to divergent mechanisms in the regulation of haematopoiesis between humans and mice^{10,11}, indicating caution needs to be excised when extrapolating results between the two species. Therefore, an accessible human system that recapitulates the key events of embryonic haematopoiesis will be an important tool for

¹Murdoch Children's Research Institute, The Royal Children's Hospital, Parkville, VIC, Australia. ²Department of Paediatrics, Faculty of Medicine, Dentistry and Health Sciences, University of Melbourne, Parkville, VIC, Australia. ³The Novo Nordisk Foundation Center for Stem Cell Medicine (reNEW), Murdoch Children's Research Institute, Parkville, VIC, Australia. ⁴Cancer Immunology Program, Peter MacCallum Cancer Centre, Melbourne, VIC, Australia. ⁵Sir Peter MacCallum Department of Oncology, The University of Melbourne, Parkville, VIC, Australia. ⁶Present address: Changping Laboratory, Beijing, China. ⁷These authors contributed equally: Shicheng Sun, Ali Motazedian. ⁸These authors jointly supervised this work: Andrew G. Elefanty, Edouard G. Stanley.

 e-mail: scsun@cpl.ac.cn; ed.stanley@mcric.edu.au

understanding blood and immune cell development from a human perspective. Such a system would also facilitate the de novo generation of immune cells with potential clinical applications.

Differentiation of human PSCs has enabled the generation of haematopoietic cells in vitro^{12,13}. However, PSC-derived haematopoietic cells often resemble those derived from extra-embryonic haematopoiesis in the yolk sac, a transient wave of haematopoiesis in the early embryo which predominantly contributes to erythroid and myeloid lineages^{12–14}. By contrast, intra-embryonic definitive haematopoiesis, arising from the dorsal aorta within the aorta–gonad–mesonephros (AGM), gives rise to multi-lineage development encompassing erythroid, myeloid, and lymphoid cells^{4,6,8}. Despite many attempts^{15–18}, differentiation of PSCs to AGM-like haematopoiesis has been challenging, primarily because embryonic data corresponding to this developmental stage has been limited. In this context, recent spatial and single-cell transcriptomic analyses of human embryos have been highly illuminating^{19,20}. This data argues that AGM haematopoiesis is built upon haemogenic endothelial cells with a distinct arterial gene profile and provides a touchstone for deriving AGM-like haematopoiesis from PSCs in vitro.

Studying lymphoid commitment in vitro is an additional challenge, an event that is highly dependent on NOTCH ligands. In vitro lymphopoiesis, from either primary human haematopoietic progenitors or PSCs, requires an exogenous supply of NOTCH ligands provided by immobilized recombinant proteins^{21–23}, or ectopic expression by mouse stromal cells, such as OP9 or MS5^{24–27}. Additionally, the relative opacity of many in vitro PSC differentiation platforms not only impacts the reproducibility of these methods, but also affects the exact type of cells that are generated. In turn, this lack of clarity also raises concerns about manufacturing lymphoid cells from PSCs for clinical applications, which may result in variable treatment outcomes. Nevertheless, there are many protocols that generate lymphoid cells from PSCs in vitro²⁸. A number of these methods focus on natural killer (NK) cells, generating cells that display effective cell-killing activity and show promise for biomedical applications^{29,30}. In the case of PSC-derived NK cells, it is likely such cells arise from a population that resembles yolk-sac-derived erythroid-myeloid progenitors^{31,32}. Indeed, Dege et al.³¹ identified at least two distinct developmental pathways for NK generation from PSCs that were independent of haematopoietic stem cell (HSC) development, giving rise to either CD56dim or CD56bright NK cells.

Analysis of differentiating human CD34+ progenitors indicates that CD13+ myeloid intermediates, when provided with appropriate environmental cues, including co-culture with stromal cells or in the presence of stromal cells and/or hydrocortisone robustly generate cells resembling CD56dim NK subsets³³. This conclusion is also supported by studies from Chen and colleagues³⁴, who showed that human peripheral blood-derived myeloid progenitors could also generate NK cells. These examples provide a counterpoint to well-established pathways for the generation of innate lymphoid cells, including NK cells, reviewed elsewhere^{28,35}. Taken together, further work is required to understand the many potential developmental pathways with which innate lymphoid cells (ILCs), including NK cells, are generated during embryogenesis.

Our previous work showed that PSC-derived haematopoietic organoids containing DLL4+ endothelial cells could prime haematopoietic progenitors to the lymphoid lineage^{18,36}. However, the frequency of DLL4+ endothelial cells and the restricted organoid structure limited the extent of lymphoid differentiation. In this study, we developed a monolayer differentiation method that robustly generated NOTCH ligand-expressing arterial and haemogenic endothelial cells, whose gene profile resembled that of arterial haemogenic endothelial cells found in the AGM. Our results show that our PSC-based AGM-like haematopoiesis recapitulated a series of events associated with early human haematopoiesis and lymphopoiesis, enabling

the efficient generation of NK cell progenitors that arise from a defined lymphoid developmental pathway.

Results

Efficient generation of arterial endothelial cells (AECs) and haematopoiesis in vitro

Combining attributes of protocols designed to generate intra-embryonic mesoderm and haemogenic endothelium^{15,18,36,37}, we developed a method that robustly generated DLL4-expressing AECs (Fig. 1a). Patterning differentiating PSCs over the first two days resulted in the rapid transit of cells through stages indicative of *MIXL1*+ primitive streak (day 1)³⁸ and CD13+ early mesoderm (day 2). Treatment of this mesoderm population with BMP4 whilst simultaneously inhibiting Activin signalling (A8301) resulted in the generation of cells highly enriched for expression of the mesodermal-endothelial markers CD13 and KDR (day 3) (Supplementary Fig. 1a–c). On day 6, the CD34+ population ($80 \pm 2\%$, mean \pm SEM, $n = 31$ experiments) in differentiation cultures uniformly co-expressed the AEC markers VE-cadherin, CXCR4 and DLL4 (Fig. 1b–d). Importantly, this method for generating AECs was reproducible across nine different human iPSC lines or ESC lines (Fig. 1d and Supplementary Fig. 1d), with one PSC giving rise to approximately six CD34+ DLL4+ cells (Supplementary Fig. 1e). On day 6, the confluent endothelial cell monolayer was passaged to enable further expansion or in preparation for cryopreservation, the latter option providing a significant logistical advantage of this method (Supplementary Fig. 1f). Between day 6 and day 12, cells proliferated further to re-establish a confluent monolayer and began to produce haematopoietic cells.

By day 12, CD34+ CD43+ haematopoietic progenitor cells represented a substantial fraction of the culture, as assessed by flow cytometry (Fig. 1e). Over the ensuing 3 days, CD45+ blood cells begin to upregulate expression of the lymphoid lineage marker CD7, in response to the introduction of IL7 into the culture medium (Fig. 1e). On day 15, using *RAG1*:GFP reporter lines³⁶, we detected a small fraction of *RAG1*+ cells within the CD34+ CD7+ haematopoietic cell population (Fig. 1e, f). The frequency of this *RAG1*+ population increased over the next four days, an increase that was accompanied by the down-regulation of CD34 (Fig. 1e, f). Fluorescence images also showed an accumulation of *RAG1*:GFP+ cells from day 15 to day 19, suggestive of ongoing lymphoid differentiation (Fig. 1g). At day 23, the majority of CD7+ cells were negative for *RAG1* but positive for CD161 (KLRB1), a cell surface marker frequently associated with innate lymphoid cells (Fig. 1h, i). Indeed, approximately half of the CD161+ cells also expressed the NK cell marker CD56. Additional experiments with two independent iPSC lines, PB1 and PB5, showed each input iPSC yielded 35 ± 3.1 , and 59 ± 17 CD161+ CD7+ cells for cultures in which IL15 was added at day 15, and 7.3 ± 2.3 and 12 ± 1.8 CD161+ CD7+ cells for cultures when IL15 was added at day 19 (average \pm S.E.M for three technical replicates—see source data file). Collectively, these results show that our DLL4-expressing arterial haematopoietic culture (AHC), designated AHC, efficiently generates lymphoid cells with characteristics of the ILC lineage. This process occurs without the requirement for exogenously added NOTCH ligands, which is a mandatory characteristic of previously described lymphoid differentiation methods.

PSC-derived AHC models human embryonic haematopoiesis

To explore the differentiation trajectories of cells subjected to this protocol, we performed time-series single-cell RNA-sequencing (scRNA-seq) analysis of AHCs at day 6, day 12, day 15, day 19, and day 25 (haematopoietic cells only on day 25), encompassing the period from the generation of haemogenic endothelium to lymphoid commitment (Supplementary Fig. 2a). The results from this experiment were cross-mapped to a recently reported dataset derived from early human embryonic haematopoietic tissues, including the AGM and the foetal liver (Fig. 2a and Supplementary Fig. 2a)¹⁹.

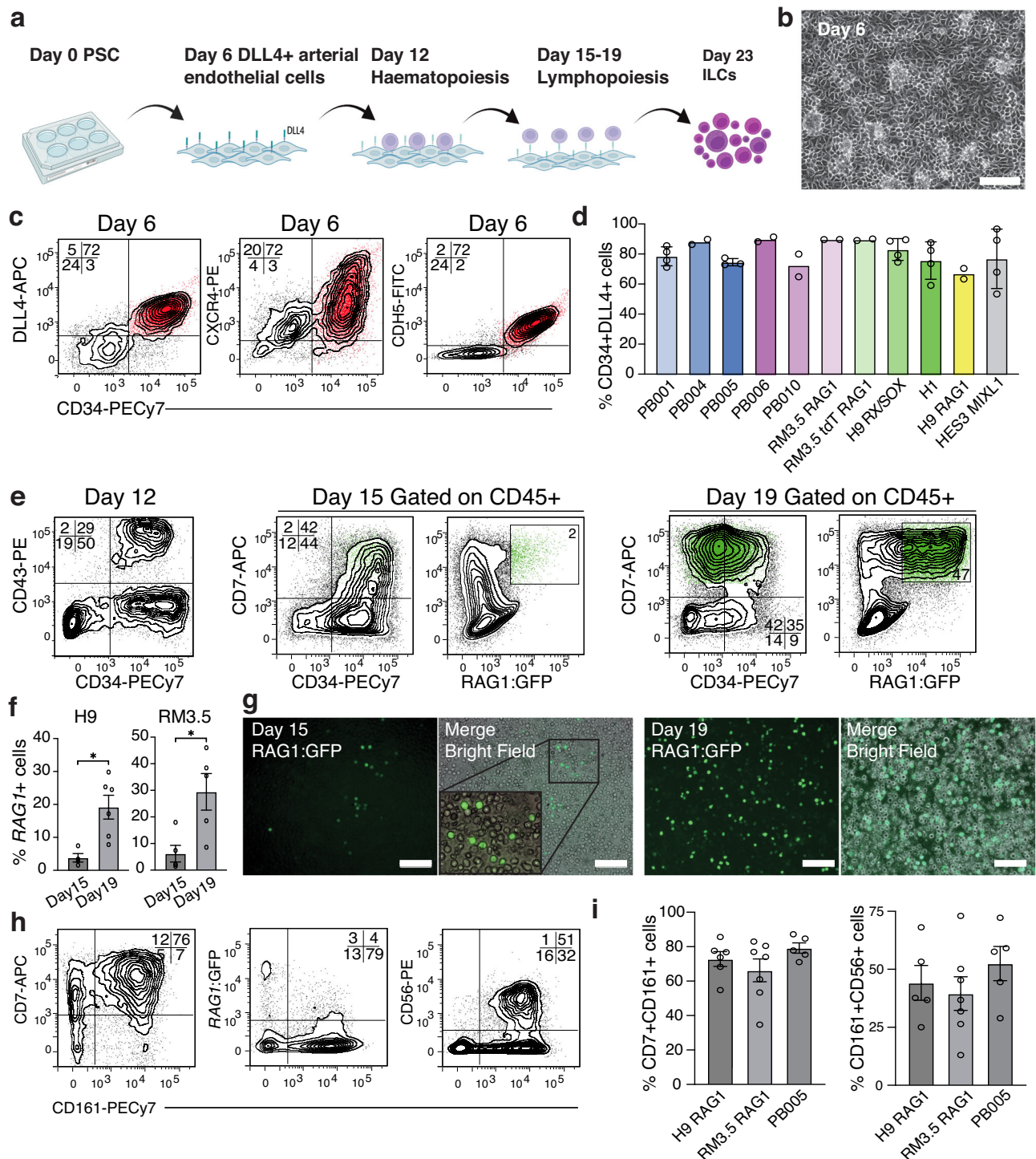


Fig. 1 | Differentiation of PSCs to DLL4+ AECs and lymphoid haematopoietic cells. **a** Sequential stages of PSC differentiation towards DLL4+ AECs, haemogenic endothelium, haematopoietic progenitors, lymphoid commitment, and ILCs at the approximate corresponding days. Created with BioRender.com released under a Creative Commons Attribution-NonCommercial-NoDerivs 4.0 International license (<https://creativecommons.org/licenses/by-nc-nd/4.0/deed.en>). **b** Bright-field (BF) image of day 6 monolayer cell culture. Scale bar, 100 μ m. **c** Flow cytometry analysis of day 6 cultures showing co-expression of the AEC markers DLL4, CXCR4, and CDH5 on CD34+ cells. Red dots indicate CD34+ DLL4+ cells. **d** Bar graph summarizing flow cytometry analysis of CD34+ DLL4+ expression in day 6 samples representing independent experiments using nine distinct parental PSC lines (and two subclones of RM3.5 iPSCs and H9 ESCs). Data is shown as the mean \pm SD for ≥ 3 independent experiments, otherwise, only the mean is shown. **e** Flow cytometry analysis tracing progressive differentiation from CD43+ CD34+ HSPCs (day 12), to

CD34+ CD7+ lymphoid progenitors (day 15), to CD34- CD7+ and CD7+ RAG1+ lymphoid cells (day 19). Green dots indicate RAG1:GFP+ cells. **f** Quantification of RAG1:GFP+ cells showing the frequency of RAG1+ cells increases from day 15 to day 19. Statistics were calculated by a two-sided *t*-test; data shown as mean \pm SEM; *n* = 5 for RM3.5 day 15, *n* = 5 for RM3.5 day 19, *n* = 4 for H9 day 15, *n* = 6 for H9 day 19. *P* (H9) = 0.0105, *P* (RM3.5) = 0.0152. The *n* values designate independent experiments. **g** Bright field and fluorescence images showing RAG1:GFP cells at day 15 and day 19. Scale bar, 100 μ m. **h** Flow cytometry of CD45+ cells at differentiation day 23 showing expression of CD7, CD161 and RAG1, and the NK cell marker CD56. **i** Frequency of the CD7+ CD161+ innate lymphoid cells and CD161+ CD56+ NK-like cells in independent experiments using three distinct PSC lines (mean \pm S.E.M.). For the values in the left (L) and right (R) panels, these are *n* = 5 (L) and 6 (R) for H9, *n* = 7 (L) and 7 (R) for RM3.5, *n* = 5 (L) and 5 (R) for PB005, (for Fig. 1d, f, and i, *n* = number of independent experiments). Source data are provided as a Source Data file. Frequencies of each cell fraction is indicated.

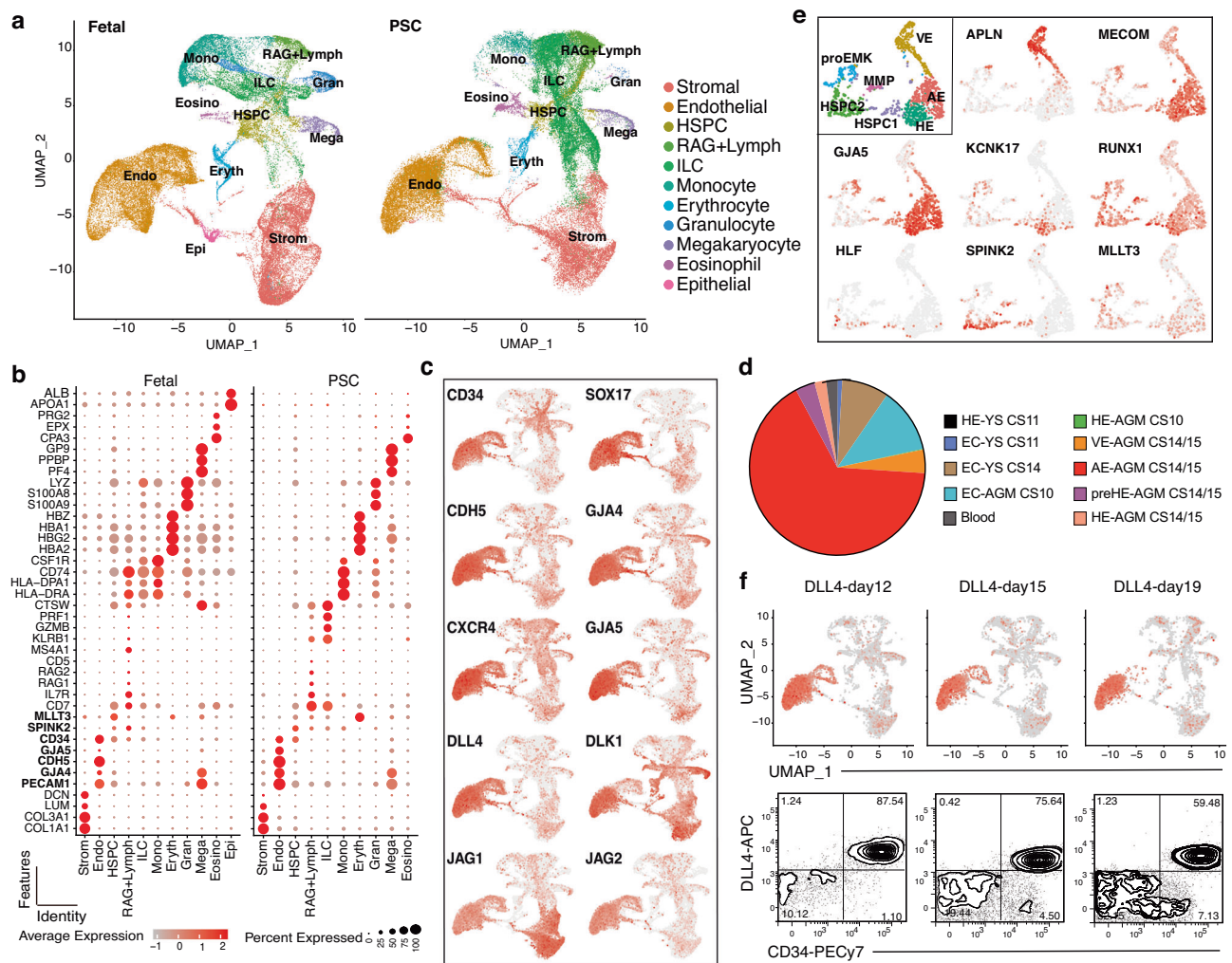


Fig. 2 | scRNA-seq reveals AEC and haematopoietic differentiation resembles human AGM and foetal liver haematopoiesis. a UMAP projection showing a comparison between cells isolated from the AGM and foetal liver (left)¹⁹ and cells generated by PSC differentiation in vitro (right). Stromal cell strom, endothelial cell Endo, haematopoietic stem/progenitor-like cell HSPC, lymphoid progenitor expressing RAG genes RAG+ lymph, innate lymphoid cells ILC, monocyte mono, erythroid cells Eryth, granulocyte Granu, megakaryocyte Mega, eosinophils Eosino, epithelial cells Epi. **b** Dot plots showing differentially expressed genes of haemogenic and haematopoietic cells from PSC (right) and from foetal tissues (left). **c** UMAP showing the expression of AEC associated genes (*CD34*, *SOX17*, *CDH5*, *GJA4*,

CXCR4, and *GJA5*), and NOTCH ligand genes (*DLL4*, *DLK1*, *JAG1*, and *JAG2*) on PSC-derived cells in vitro. **d** Transcriptomics-based ACTINN prediction showing in vitro PSC-derived endothelial cells within the endothelial cell cluster projected to the AECs collected from the AGM of CS14/15 embryos (AE-AGM CS14/15). **e** UMAPs showing the expression of key genes related to endothelial-to-haematopoietic transition and haemogenic endothelial cells in the fraction of day 12 and day 15 *CD34*⁺ *CDH5*⁺ *RUNX1*⁺ cells. **f** UMAPs (upper panel) and flow cytometric validation (lower panel) show the persistent expression of *DLL4* on *CD34*⁺ endothelial cells on day 12, day 15 and day 19. Source data are provided as a Source Data file.

This comparative analysis indicated that our in vitro PSC differentiation method generated a diverse spectrum of cell lineages that mirror those arising during early human intraembryonic haematopoiesis in vivo (Fig. 2a, b). Consistent with this, cells within our cultures expressed members of the *HOXA* cluster, including *HOXA9* (Supplementary Fig. 2b), which has been previously associated with intraembryonic mesoderm and AGM haematopoiesis^{18,19}. The spectrum of cells found within our monolayer cultures includes fibroblast-like stromal cells (*COL3A1* and *COL1A1*), AECs (*CDH5* and *PECAM1*), haematopoietic stem/progenitor cell-like cells (HSPCs) (*CD34*, *SPINK2*, and *MLLT3*), erythroid cells (*HBZ*, *HBA1*, and *HBA2*), a variety of myeloid haematopoietic lineages, and lymphoid lineages marked by *RAG* genes or ILC-associated genes (Fig. 2a, b and Supplementary Fig. 2h).

The potential of progenitors suggested by single-cell RNAseq analysis was investigated by supplementing day 12 cultures with growth factors capable of supporting the development of other lineages or by transferring day 12 cells into conditions enabling T and B

lymphoid development. These experiments showed that supplementing cultures with EPO or MCSF led to the generation of *CD235a*⁺ erythroid and *CD14*⁺ myeloid cells, respectively (Supplementary Fig. 2c). Transfer of day 12 haematopoietic cells to *MSS*³⁹ or *OP9-DLL4*⁴⁰ stromal co-culture systems enabled the development of *CD3*⁺ *TCR*⁺ T cells (*TCR*⁺, 33 ± 9.8%, four experiments), *RAG1*⁺ *CD19*⁺ *CD10*⁺ B lymphoid lineage cells (Supplementary Fig. 2d). Further experiments in which day 23 haematopoietic cells were embedded in *DLL4*-*MSS* artificial thymic organoids (ATOs)^{24,25} showed the development of naïve single positive *CD8* (and to a lesser extent, *CD4*) T cells which expressed *CCR7* and *CD45RA* (Supplementary Fig. 2e). Stimulation of these single positive populations with anti-*CD3* and anti-*CD28* antibodies resulted in levels of proliferation similar to that reported previously for T cells derived from other differentiation protocols²⁵. Last, disaggregation of day 6 cultures and re-seeding of cells in Matrigel revealed the capacity of cells to form tubes, suggestive of a bone fide endothelial identity (Supplementary Fig. 2f). Collectively, these experiments indicated our cultures

could generate a broad spectrum of lineages, including some of those identified by RNAseq analysis.

On day 25, cultures contained predominantly lymphoid cells, an outcome we attribute to the provision of IL7 and IL15 as the key haematopoietic cytokines over the prior 6 days. Importantly, our analysis showed that PSC-derived endothelial cells expressed a cohort of AEC-associated genes, including *SOX17*, *GJA4*, *CXCR4* and *GJA5* (Fig. 2c). Based on transcriptomic features, ACTINN⁴¹, an artificial intelligence-based computation program, predicated that these endothelial cells resemble the AECs found in the AGM of Carnegie stage (CS) 14/15 human embryos (Fig. 2d). Consistent with this prediction, we detected activation of specific arterial-haemogenic genes, such as *MECOM* (*EVII*), *KCNK17*, and *SPINK2* (Fig. 2e). Additionally, these AECs expressed a group of NOTCH-ligand genes, including *DLL4*, *DLK1*, *JAG1*, and *JAG2* (Fig. 2c). Flow cytometry and immunofluorescence validated protein expression of these genes (Fig. 2f and Supplementary Fig. 2g, i). We found CD34⁺ cells persistently expressed DLL4 from day 6 to day 19, creating conditions favourable for lymphopoiesis (Fig. 2f). Interestingly, although JAG1 was expressed by both endothelial cells and stromal cells, its endothelial expression gradually diminished from day 6 to day 19 (Supplementary Fig. 2i). In the human embryo dataset, JAG1⁺ cells were more prevalent in the AGM-AEC population of early embryos, while fewer JAG1⁺ AECs were found in the foetal liver (Supplementary Fig. 2j, k), suggesting that JAG1 expression, instead of DLL4, may be an important indicator of arterial specification in the AGM. Ligand-receptor pair analysis, using CellChat⁴², suggested endothelial cells within these cultures may represent a major source of NOTCH ligands, signalling to NOTCH1⁺ haematopoietic progenitors and lymphoid cells (Supplementary Fig. 2l). Collectively, these results suggest our PSC-derived endothelial cells acquire a cellular identity that closely resembles AECs present at a stage of human embryogenesis during which intra embryonic haemopoiesis is initiated.

Lymphoid commitment and lineage specification

The widespread endogenous expression of NOTCH-ligands by our culture system provides an environment conducive to lymphoid commitment. As such, we focused our analysis on the emergence of lymphoid cell populations within the haematopoietic cell pool (Fig. 3a and Supplementary Fig. 3a). UMAP clustering of scRNA-seq data showed that although this pool included a small fraction of haematopoietic progenitor cells and myeloid cells, the vast majority of cells belonged to the lymphoid lineages (Fig. 3a–c). Time series analysis showed that myeloid compartments emerged on day 12, earlier than the wave of lymphoid commitment on day 15 (Fig. 3b). This analysis also captured three transient lymphoid progenitor populations; lymph_pro1 on day 15, and lymph_pro2 and lymph_pro3 on day 19 (Fig. 3b). By day 25, ILC-like cells (*KLRB1*, *NKG7*, and *GZMB*) and T cell progenitors (*RAG1*, *CD5* and *TCF7*) were the predominant cell types; both populations included a sub-fraction enriched with cell-cycle related genes (*CDK1*, *MKI67*, and *CENPF*) (Fig. 3b, c). However, we did not detect cells representing the B cell lineage (Supplementary Fig. 3b), reminiscent of observations of human foetal liver haematopoiesis, where the NK/ILC and T cell lineages emerge together as a separate branch of lymphopoiesis from that giving rise to B cells⁴³. The results of pseudo-time analysis using Monocle were consistent with our real-time analysis (Fig. 3b), suggesting our dataset could be used to address other questions relating to the dynamics and kinetics of the lymphoid differentiation process.

Cluster-specific gene expression distinguished the three lymphoid progenitor populations (Fig. 3c and Supplementary Fig. 3c, d). Lymph_pro1 upregulated *NOTCH1* and *CD7* but downregulated *CD34*, indicative of lymphoid commitment. Retained expression of the stem cell gene, *SPINK2*, on lymph_pro1 also distinguished this population from lymph_pro2 and lymph_pro3. Lymph_pro2 showed a high-level expression of the IL7 receptor gene (*IL7R*) and an upregulation of the NOTCH-

pathway genes, *NOTCH1* and *HES4*. However, lymph_pro3 showed downregulation of *IL7R* but increased expression of *KLRB1*, which may suggest a cell fate potentially directed towards an ILC-like phenotype. Furthermore, analysis of a cohort of T cell differentiation genes indicated the lymph_pro2 and lymph_pro3 clusters showed characteristics consistent with differentiation trajectories towards T cell lineage and the ILC lineage, respectively (Fig. 3d). The transcription factors *BCL11B* and *TCF7*, key drivers of T cell commitment, were enriched in lymph_pro2 and T cell progenitors, consistent with the expression patterns of *RAG1*, *RAG2*, and *PTCRA*. Additionally, the elevated expression of IL7R in lymph_pro2 and T progenitor clusters, but not in lymph_pro3 and ILC populations, suggests IL7 signalling might be important for ILC vs T cell lineage specification.

To further characterise the ILC-like populations, we regressed cell-cycle-related genes and clustered for cell type annotation. This analysis showed the ILC-like cells could be subdivided into three clusters: NK/ILC1a, NK/ILC1b, ILC2-like cells (Fig. 3e). All ILC-like cells expressed *NKG7* and *KLRB1*, while the NK/ILC1 groups expressed typical genes encoding cytotoxic proteins, including perforin (*PRF1*), granzyme B (*GZMB*), granzysin (*GZLY*), as well as the NK cell surface marker gene NCAM1/CD56 (Fig. 3f and Supplementary Fig. 3e). However, the ILC2-like cells expressed *PTGDR2* and *IL7R*, suggesting that the IL7 signalling might be also important for further sub-lineage specification within ILC compartment.

Collectively, these results suggest that our arterial haemogenic culture system expressing intrinsic NOTCH-ligands efficiently patterned lymphoid lineages, in which *IL7R* was shown to be a differential marker for different lymphoid progenitors and their committed progeny.

IL7 regulates T vs NK cell lineage commitment

Consistent with results summarised in the dot and violin plots in Fig. 3c, d, UMAP projections showed that the pattern of *IL7R* expression contrasted with that of *KLRB1* (CD161), and that clusters enriched with *RAG1* and *CD4* also expressed a higher level of *IL7R* (Supplementary Fig. 4a). Analysis of the entire AHC did not detect *IL7* transcripts (Supplementary Fig. 2b), facilitating dissection of the consequences of IL7 supplementation on differentiation outcomes. Therefore, we titrated the concentration of IL7 and examined how this influenced the appearance of different lymphoid populations that expressed the IL7 receptor. For these experiments, we also removed IL15 from the AHC because of its defined function in supporting human NK cell differentiation⁴⁴.

Using the *RAG1*:GFP PSC reporter line³⁶, we examined 4 concentrations of IL7 (0 ng/ml, 0.1 ng/ml, 1 ng/ml, and 20 ng/ml) from day 12 to day 23, spanning a period between the emergence of haematopoietic progenitors and lymphoid lineage commitment. Flow cytometry analysis showed that IL7 was not necessary for the generation of CD7⁺ cells or *RAG1*:GFP⁺ cells, suggesting this cytokine is dispensable for haematopoietic progenitors to commit to the lymphoid lineage (Fig. 4c). Nevertheless, the addition of even low concentrations of IL7 (0.1 ng/ml) significantly increased the frequency of CD7⁺ cells. Conversely, increased IL7 concentrations reduced the frequency of IL7R⁺ cells; the highest IL7 concentration (IL7-hi, 20 ng/ml) completely blocked the generation of CD7⁺ lymphoid cells with surface expression of IL7R, whilst the lowest IL7 concentration (IL7-lo, 0.1 ng/ml) produced cultures with the highest frequency of IL7R⁺ lymphoid cells. These latter results are consistent with previous findings showing IL7 downregulates the surface expression of its receptor^{45,46}.

The addition of IL7 increased the frequency of *RAG1*⁺ CD161[−] cells and the *RAG1*[−] CD161⁺ population, representing the T and the innate lymphoid lineages, respectively (Fig. 4b). Importantly, IL7 was required to upregulate *RAG1*:GFP expression, which reflects *RAG1* mRNA levels³⁶, confirming IL7 as an important driver of lymphoid differentiation (Fig. 4b and Supplementary Fig. 4c). We also examined CD4 and CD8a expression as markers of further commitment to the T

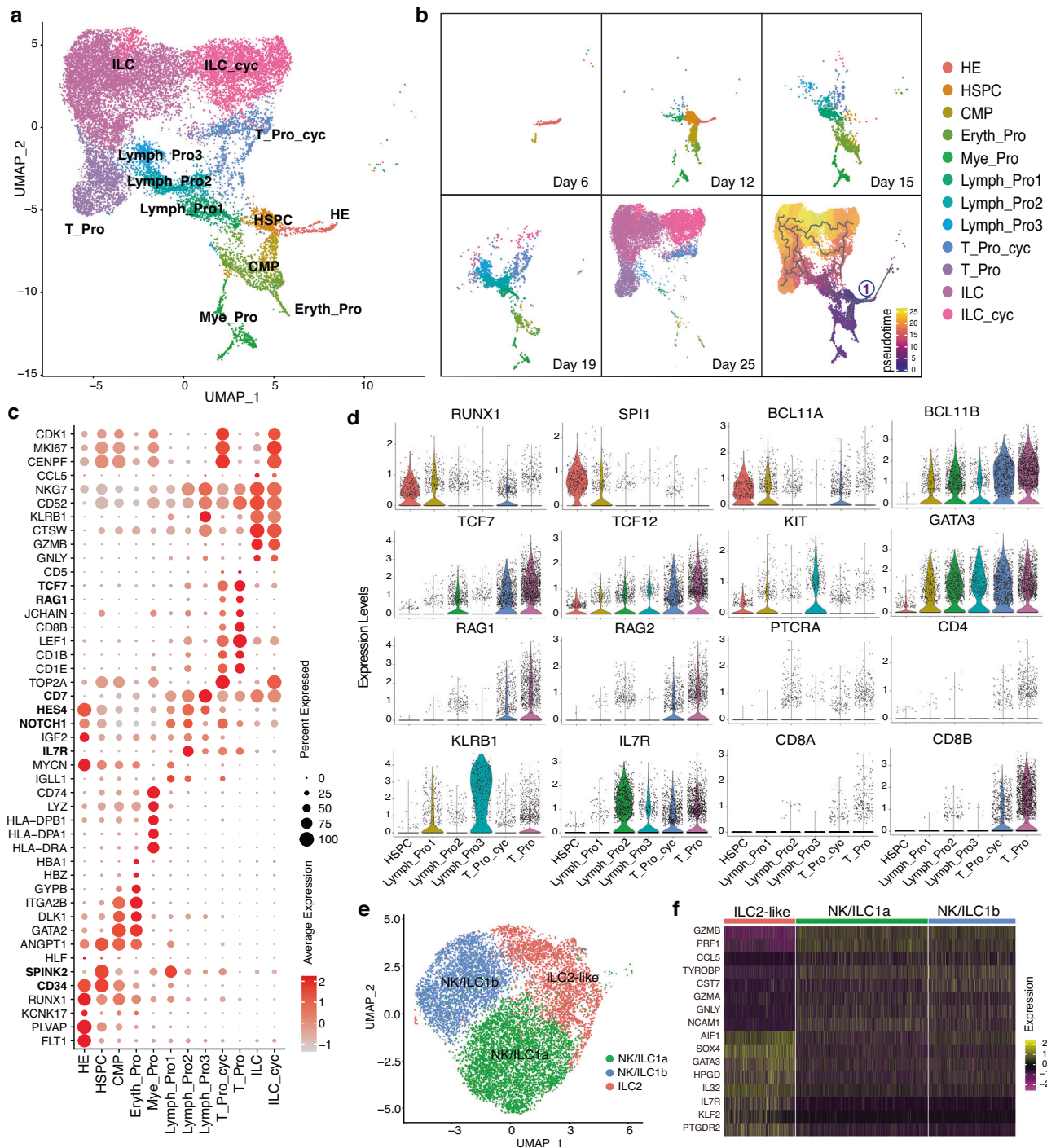
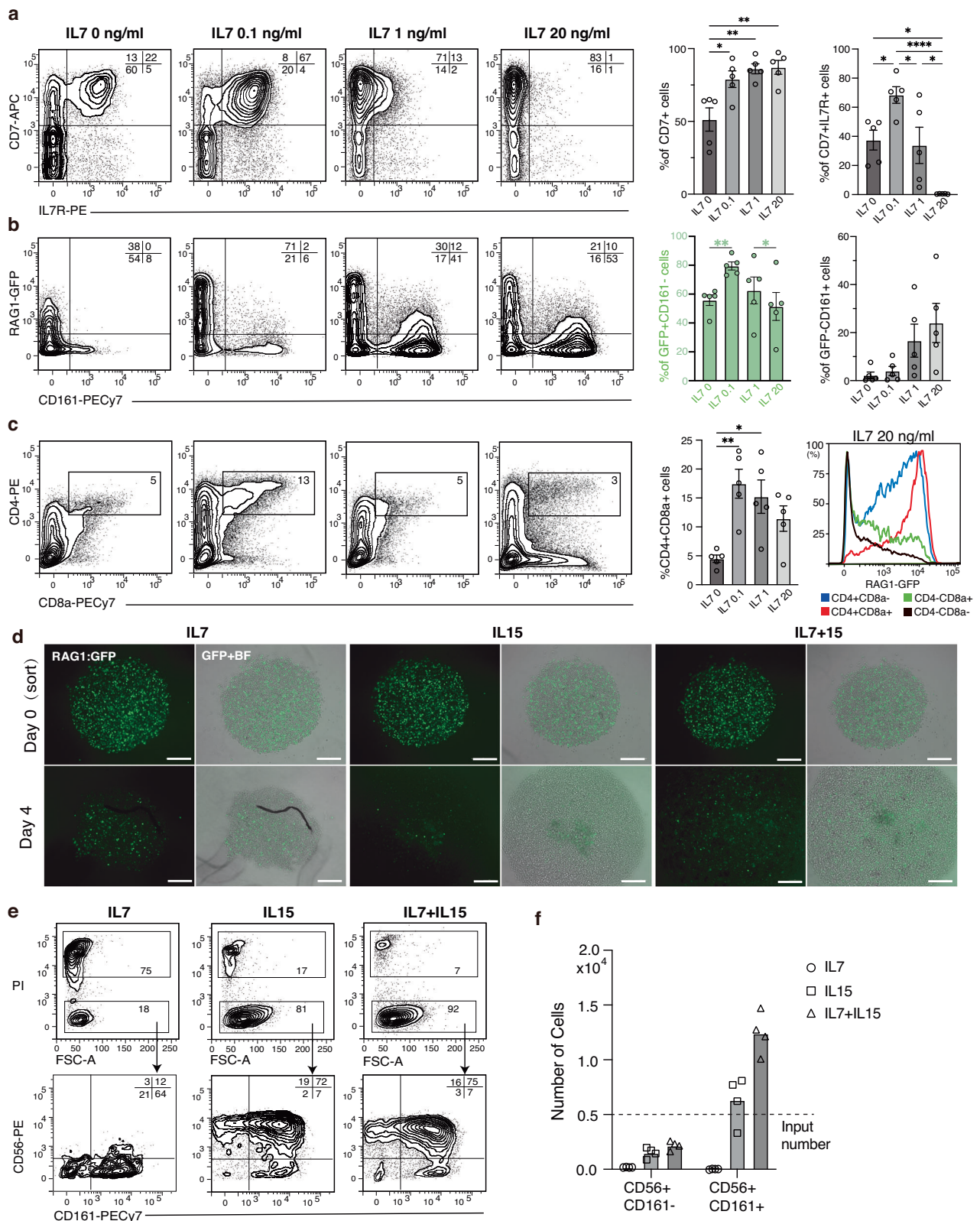


Fig. 3 | Lymphoid cell development in the PSC-derived AHC. a UMAP projection showing haematopoietic cell types in the PSC-based AHC. Cells representing hematopoietic cell clusters in Fig. 2a. Haemogenic endothelial cells HE, haematopoietic stem/progenitor-like cells HSPC, common myeloid progenitor-like cells CMP, erythroid progenitors Eryth_Pro, myeloid progenitors Mye_Pro, three lymphoid progenitor populations (Lymph_Pro1, Lymph_Pro2, and Lymph_Pro3), T cell progenitor (T_Pro), T cell progenitor in cycling T_Pro_cyc, innate lymphoid cells ILC, innate lymphoid cells in cycling ILC_cyc. Colours indicate cell types. **b** UMAPs show

the development of haematopoietic cell types in real-time (day 6, day 12, day 15, day 19, and day 25) and in pseudo-time. Colours indicate cell types. **c** Dot plot showing differentially expressed genes distinguishing cell types generated in the PSC-based AHC. **d** Violin plot showing the expression of a cohort of genes associated with T cell fate commitment. **e** UMAP showing three sub-clusters within the ILCs: NK-ILC1-like cells a (NK/ILC1a), NK-ILC1-like cells b (NK/ILC1b), and ILC2-like cells (ILC2-like). **f** Heatmap depicting the relative expression levels of selected genes defining the identity of the indicated cell types. Source data are provided as a Source Data file.

cell lineage. We found the IL7-lo conditions promoted the generation of CD4⁺ CD8a⁺ double-positive cells that emerged from the immature CD4⁺ single positive population (Fig. 4c). Moreover, these conditions did not generate an atypical immature CD8a⁺ single positive population which is often observed in in vitro T cell differentiation systems²⁵, but rarely seen in thymopoiesis in vivo. In this regard, IL7-lo conditions

generate a cell profile that more closely resembles early T cell differentiation in the human thymus. Indeed, like in vivo thymopoiesis, we found that CD4⁺ CD8a⁺ cells showed the highest level of *RAG1* expression⁴⁷. Of the remaining fractions, CD4⁺ CD8a⁻ cells showed the next highest level of *RAG1* expression, while the CD4⁺ CD8a⁺ and CD4⁺ CD8a⁻ populations showed minimal levels of *RAG1*. Interestingly,



analysis of our scRNA-seq data suggested that *RAG1*-hi cells were enriched with T cell-associated genes, while *RAG1*-lo cells showed expression of NK cell-related genes (Supplementary Fig. 4d). Collectively, these results support the conclusion that lymphoid differentiation within our AHC system is highly sensitive to IL7 concentrations and reaffirms that high levels of IL7 favour the development of innate lymphoid lineages⁴⁸. Importantly, the highly defined

nature of the AHC system provides myriad opportunities to dissect key events in lymphoid lineage commitment and differentiation.

NK cells generated from *RAG1*⁺ and early lymphoid progenitor cells

In the above experiments, we observed CD161⁺ *RAG1*⁺ cells in the IL7-hi condition, prompting us to investigate whether human *RAG1*⁺ cells

Fig. 4 | IL7 is a determinant factor of fate choices between the T and the ILC lineages. **a** Flow cytometry analysis of CD7 and IL7R (left) expression with quantification of frequencies (right) showing IL7 increases the frequency of CD7+ cells but higher concentrations of IL7 reduce the percentage of CD7+ IL7R+ cells. Left graph p (0 vs 0.1) = 0.0162, (0 vs 1) = 0.0027, (0 vs 20) 0.0021; right graph: p (0 vs 0.1) 0.0498, (0.1 vs 1) = 0.0259, (1 vs 20) = 0.0327, (0.1 vs 20) < 0.0001, (0 vs 20) = 0.0168. **b** Flow cytometry examination of CD7+ population for CD161 and *RAG1*:GFP (left) expression with quantifications of frequencies (right) showing IL7 increased the percentage of CD161+ *RAG1*+ cells committed to the T lineage and CD161+ *RAG1*- cells committed to the ILC lineage. Left bar graph p (0 vs 0.1) = 0.0078, (1 vs 20) = 0.0350. **c** Flow cytometry examination of the expression of CD4 and CD8a (left) with quantifications of frequencies (right) showing 0.1 ng/ml IL7 is optimal for generating CD4+ CD8a+ double-positive T cell precursors. Bar graph showing different levels of *RAG1*:GFP expression across the four populations

marked CD4 and/or CD8a. p (0 vs 0.1) = 0.0039, (0 vs 1) = 0.0167, (**a–c**, a bar graph is shown in mean \pm SEM, statistics is calculated by a one-way ANOVA test, $n = 5$ independent of experiments). **d** Fluorescent and BF images showing GFP+ cells on the day of sorting and replating (day 0, sort) and after four days in culture (day 4) under the indicated conditions supplemented with IL7 (20 ng/ml), IL15 (20 ng/ml), or IL7 + IL15 (both 20 ng/ml). **e** Flow cytometry plots show that IL15 (20 ng/ml) and IL7 + IL15 (both 20 ng/ml) support cell growth and the generation of CD161+ CD56+ NK-like cells but IL7 (20 ng/ml) does not. **f** Quantification of output cell numbers per 5000 input *RAG1*:GFP+ cells (as normalized to 1) showing IL7 + IL15 robustly supported the generation of CD161+ CD56+ NK-like cells from *RAG1*+ lymphoid progenitors. Bar graphs show the mean of data points derived from 2 independent experiments ($n = 2$) each comprising two technical replicates. Source data are provided as a Source Data file.

could give rise to cells of the NK ILC lineage⁴⁹. On day 19 when AHCs were enriched with *RAG1*-low cells (Supplementary Fig. 4e), we separated haematopoietic cells from the AHC and purified GFP+ cells using FACS. The sorted GFP+ cells were cultured in a medium supplemented with IL7, IL15, or both factors, at 20 ng/ml. Examining these cultures after four days revealed that IL7 alone could not support continued cell growth, while IL15 alone, and IL7 together with IL15 promoted an increase in cell numbers (Fig. 4d and Supplementary Fig. 4f). Flow cytometry analysis showed that these latter two conditions yielded a high frequency of CD161+ CD56+ *RAG1*-NK-like cells, with each GFP+ input cell giving rise to 1.2 ± 0.2 (IL15) and 2.4 ± 0.2 (IL7 + IL15) CD161+ CD56+ NK-like cells after four days (Fig. 4e). These results indicate that human *RAG1*+ lymphoid progenitors can efficiently generate NK-like cells.

Given the expansion of lymphoid-derived NK cells in response to IL7 and IL15, we next examined if these same conditions were able to generate NK cells from haematopoietic progenitors that arise at earlier stages of our AHC system, without a requirement for prior enrichment of progenitors using FACS. Capitalising on the high frequency of CD7+ CD34+ lymphoid progenitors at day 15, we separated suspension cells from the AHC on this day and cultured these cells in media supplemented with only IL7 and IL15. On day 20, flow cytometry analysis showed the efficient generation of CD161+ CD56+ cells (Supplementary Fig. 4g) was also accompanied by a reduced number of *RAG1*+ cells. Notably, after only 5 days of IL15 treatment these cells possessed a rudimentary cytotoxic function (Supplementary Fig. 4h) that was comparable to cells isolated from peripheral blood (PBMCs). Extending the time in which cells were exposed to IL15 for a further 15–17 days (from day 15) enabled further maturation of this population, evidenced by the up-regulation of CD16 on CD161+ cells, a phenotype conventionally associated with enhanced cytotoxicity (Supplementary Fig. 4i). Consistent with this, cells from cultures subjected to 15 or more days of IL15 treatment exhibited an ability to kill K562 erythroleukemia cells (~50% after 4 h at an Effector: Target ratio of 8:1 or ~40% for ratios of 4:1) that was comparable with that reported for both donor-derived or iPSC derived NK populations reported in the literature^{29,31,50,51} (Supplementary Fig. 4j). Taken together, these data strongly support the proposition that CD161+ CD56+ cells generated via our AHC culture system represent early cells of the NK cell lineage.

Discussion

In this study, we report a human AHC system, representing a simple and efficient method to study and model human embryonic haematopoiesis/lymphopoiesis in vitro. The critical characteristic of this system is the generation of a lawn of NOTCH-ligand-expressing AECs which effectively directs lymphoid commitment from emerging haematopoietic progenitors. This AHC system enabled the dissection of haematopoietic cell fate determination and the identification of optimal conditions for producing human lymphoid progenitors, providing new opportunities for experimental research and medical applications.

This study provides the first time-series single-cell map of in vitro human haematopoiesis, representing a key reference for studying blood cell development. There are existing scRNA-seq datasets describing in vitro PSC-based embryonic models for the development of many organ systems, including the heart⁵², pancreas⁵³, and brain⁵⁴. Here, the development of our highly reproducible AHC system (Fig. 1c, d) has enabled the generation of a dataset that spans key stages of haematopoietic ontogeny in vitro, providing an important reference for the development of methods for blood cell production.

Detailed comparison with human embryonic and foetal tissues indicated that our endothelial cells acquired an identity that has similarities to haemogenic AECs found in the AGM region (Fig. 2a, b). In addition to classical AEC markers, previous studies show that using exogenous NOTCH ligands could specify definitive haemogenic endothelial cells during early PSC differentiation in vitro¹⁷. As such, the expression of different NOTCH ligands on our endothelial cells is also indicative of definitive hemogenic endothelial cells (Fig. 2c, f and Supplementary Fig. 2c, d). Thus, our PSC-derived haematopoietic differentiation platform generated a spectrum of blood cell types that have counterparts in the AGM and foetal liver^{19,43}, including those belonging to the erythroid, myeloid, and lymphoid lineages (Figs. 2 and 3). Although we and others have described RNAseq data sets that examine specific stages of haematopoietic differentiation^{14,19,55}, our data captures a substantial temporal window spanning ontogeny stages from endothelium to lymphoid commitment. Interestingly, we observed a rare population of cells showing the progressive expression of genes that span stages corresponding to the endothelial-to-haematopoietic transition and the formation of pre-HSCs, including *SPINK2*, *RUNX1*, *MLLT3*, *HLF*, and *MECOM(EVII)* (Fig. 2e)^{19,56}. However, the addition of IL7 at differentiation day 12 and the removal of SCF, the latter often used to promote HSPC expansion⁵⁷, most likely contributed to the observed gradual decline in the frequency of HSPCs as the cultures progressed. Nevertheless, the presence of cells at day 12 expressing pre-HSC associated markers indicates that our AHC system may be a tractable and relevant method for studying human embryonic haematopoiesis in vitro and for helping define conditions that might give rise to HSCs, a holy grail in the haematology and regenerative medicine fields.

Using the AHC system, we explored lymphoid commitment and cell fate specification between the T and the NK-ILC lineages. Without using exogenous NOTCH ligands or animal cells, mandatory components for previous lymphoid differentiation systems^{22,24–27,31}, our cultures gave rise to a primitive lymphoid progenitor marked by the expression of the stem cell gene *SPINK2* (Fig. 3c, d). The de novo appearance of this progenitor is consistent with observations from animal studies that point to the possibility of non-HSC-derived lymphoid competent precursors^{56,58–60} that contribute to early lymphopoiesis and the formation of primary lymphoid organs during embryogenesis. Furthermore, we found that IL7R expression levels foreshadowed the differing potential of progenitors to form T cell

lineages (IL7R high) or ILC lineages (IL7R low), and that levels of IL7R signalling could be manipulated to affect cell fate choices (Fig. 4a–c). Although IL7 is dispensable for early lymphoid commitment, including *RAG1* activation and CD7 upregulation, this cytokine was required for *RAG1* upregulation that further drives progenitors towards T cell development (Fig. 4c and Supplementary Fig. 4c, d). IL7 is primarily produced by stromal cells⁶¹ and low levels (>50 pg/ml) can be measured in the serum in normal or diseased states⁶². During human embryonic thymic development, the highest level of IL7 RNA expression is observed in cTEC populations), whilst thymic stromal-derived lymphopoietin (TSLP), which shares the IL7R α ⁶³, is broadly expressed at relatively low levels⁶⁴ (Human Cell Atlas). The association of IL7 expression with TEC populations places this cytokine in a position to influence key decisions in T lineage differentiation.

Our results show that the IL7R signalling network is regulated in a dose-dependent manner, with minimal levels of IL7 maintaining a level of IL7R expression required for ongoing T-cell differentiation. These results provide an example of how this AHC system can be used to dissect early lymphopoietic events and to identify optimal conditions for the efficient generation of innate and adaptive lymphoid immune cells.

We also documented an unconventional developmental pathway in which *RAG1*⁺ lymphoid cells give rise to NK cells. The *RAG* genes are responsible for gene rearrangement of antigen-specific receptors during T and B cell differentiation but are not required for the genesis of ILC lineage⁶⁵. However, experiments in mice identified an NK cell population that transiently expressed *Rag1* during development⁶⁶. Moreover, mice lacking RAG recombinase generate lymphoid NK cells with compromised fitness⁴⁹, alluding to a yet undiscovered role for *RAG1* in the genesis of the innate immune cell repertoire. Importantly, clinical reports indicate that patients with severe combined immunodeficiency caused by *RAG1* deficiency show an abnormal distribution of NK cells⁶⁷. Thus, despite caveats attached to making comparisons between the development of mouse and human immune systems, these observations, coupled with our own findings suggest grounds for further examination of the role of *RAG1* in NK cell development. In the present work, experiments using a *RAG1*:GFP PSC reporter line confirmed that, under defined conditions, *RAG1*⁺ lymphoid progenitors effectively gave rise to CD161⁺ CD56⁺ cells representing the NK cell lineage (Fig. 4d, e). Furthermore, we found that *RAG1* expression levels presaged gene expression profiles indicative of further commitment to the adaptive lymphoid lineage (*RAG1*-high) or the innate lymphoid lineage (*RAG1*-low) (Supplementary Fig. 4d). Taking the above into account, it is reasonable to speculate that *RAG1* expression may be indicative of fate decisions between different branches of the ILC lineages. Overall, our methodology provides insight into a key juncture in the genesis of innate and adaptive immunity.

Methods

Human pluripotent stem cell lines and culture

Pluripotent stem cells (PSCs) used in the study are all human origin. Work related to human pluripotent stem cell lines was conducted in accordance with RCH Human Research Ethics Committee approval 33001A. Human PSC lines, including ESCs and iPSCs, used in this study are summarized as follows: ESC H1 (male)⁶⁸, iPSC RM3.5 (male)^{RAG1:GFP36}, ESC H9 (female)^{RAG1:GFP36}, H9^{SOX17:tdTOMATO:RUXIC:GFP18}, ESC HES3 (female)^{MIXL1:GFP38}, iPSC PB0-01 (male)/-04 (female)/-05 (female)/-06 (male)/-10 (male)⁶⁹. For all differentiation experiments, we used PSCs that were less than 50 passages since their last karyotype analysis. Karyotyping was performed using the standard Infinium CoreExome-24 SNP array. Reagents for PSC culture and differentiation medium were purchased from ThermoFisher unless otherwise specified. PSC was grown in E8 medium⁷⁰ as per the manufacturer's instructions or in the

presence of inactivated mouse embryonic fibroblasts in PSC media consisting of DMEM-F12, 20% knock-out serum replacement, 1 \times non-essential amino acids, 1 \times GlutaMAX, 0.11 mM β -mercaptoethanol and FGF2 (10 ng/ml) as previously described⁷¹. Once cultures reached a confluency of approximately 80–90%, PSCs were passaged by detaching cells using dissociation buffer comprising phosphate buffer saline without calcium and magnesium (phosphate-buffered saline, PBS⁻) supplemented with 100 mM NaCl and 0.5 mM EDTA. The resultant small clumps of cells were transferred to new flasks that had been previously coated with the GeltrexTM cell culture plate coating matrix (ThermoFisher). GeltrexTM cell was dissolved in cold PBS⁻ at a dilution rate of 1:100. Cells were routinely passaged at a ratio of 1:3 to 1:5 relative to the starting flask surface area. In the case of E8 cultures, the medium was refreshed daily. For cultures containing inactivated mouse embryonic fibroblasts, the medium was changed every 2–3 days.

Monolayer differentiation of AECs and lymphoid progenitor cells from PSCs

Formulation of the basal medium is as previously described², and factors supplemented on the indicated days are listed below. On the day of differentiation, referred to as day 0, PSCs were dissociated using EDTA dissociation buffer and resuspended in day 0 medium (basal cell differentiation medium containing day 0 supplements). The cells were then plated onto Geltrex-coated 6-well plates at a low density at about 5% of confluency, approximately 10,000 cells per cm². After 26 h, the cell culture was refreshed by the day 1 medium, which was followed by an additional medium change on day 2 (after 24 h) using the day 2 medium. During day 3–6, cells were maintained in the day 3–6 medium that was replenished on day 5.

On day 6 when the culture reached confluency (over 95% coverage of the surface), the culture was dissociated using TrypLE (3 min at 37 °C) and the cells re-plated at the ratio of 1:3 onto Geltrex-coated 6-well plates as described above. From day 6–12, cells were cultured in the day 6 medium, and the medium was completely changed every 2–3 days, 2 ml/well. From day 12, the cells were cultured in day 12 medium and the medium was changed every 2–3 days. From day 19, the cells were cultured in day 19 medium and the medium was changed every 2–3 days. Flow cytometry characterization for CD161 and CD56 was performed on days 23–25. The growth factors for each day of differentiation were: Day 0: Activin A, 30 ng/ml; CHIR99021, 4 μ M; fibroblast growth factor (FGF) 2, 20 ng/ml; PIK90, 100 nM; (Y-27263 10 μ M is required for cell lines with poor viability after dissociation). Day 1: A83-01, 1 μ M; CHIR99021, 3 μ M; LDN-193189, 250 nM; FGF2, 20 ng/ml.

Day 2: A83-01, 1 μ M; vascular endothelium growth factor (VEGF), 50 ng/ml; bone morphogenic protein (BMP4), 30 ng/ml; and FGF2, 20 ng/ml. Day 3: stem cell factor (SCF), 50 ng/ml; VEGF, 50 ng/ml; BMP4, 10 ng/ml; and FGF2, 50 ng/ml. Day 6: SCF, 100 ng/ml; VEGF, 50 ng/ml; FGF2, 50 ng/ml; interleukin 3 (IL3), 10 ng/ml; and FLT3 ligand (FLT3-L), 10 ng/ml. Day 12: FLT3-L, 10 ng/ml; VEGF, 50 ng/ml; FGF2, 20 ng/ml; and IL7 1 ng/ml; Day 15: (variation only when specifically indicated *FLT3-L*, 10 ng/ml; *VEGF*, 50 ng/ml; *FGF2*, 20 ng/ml; *IL7* 20 ng/ml; and *IL15* 20 ng/ml). Day 19: FLT3-L, 10 ng/ml; VEGF, 50 ng/ml; FGF2, 20 ng/ml; IL7 20 ng/ml; and IL15 20 ng/ml.

Cytokines and small molecules

Cytokines and small molecules at each stage include (catalogue number, supplier) were, Activin A (338-AC, R&D Systems), BMP4 (314-BP, R&D Systems), FGF2 (100-18B, Peprotech), FLT3-L (300-19, Peprotech), IL3 (200-03, Peprotech), IL7 (200-07, Peprotech), IL15 (200-15, Peprotech), VEGF (100-20, Peprotech), SCF (synthesized by CSIRO), Y-27632 (72304, Stem Cell Technologies), CHIR99021 (4423, Toris), PIK-90 (SI187, Selleckchem), A83-01 (2939, Tocris), and LDN-193189 (TB6053, Tocris).

IL7 titration experiments

On day 6 of differentiation, the endothelial cell culture derived from the RM3.5^{RAG1:GFP} iPSC line was dissociated (as above) and replated onto 12-well GeltrexTM plates at the ratio of 1:3. Media for days 6–12 was as the above. From day 12, IL7 concentration was titrated based on the *Day 12 and Day 19* (as above) factors without IL15: FLT3-L, 10 ng/ml; VEGF, 50 ng/ml; FGF2, 20 ng/ml; IL7, 0/0.1/1/20 ng/ml. Media was refreshed every two days from day 12–23, and flow cytometry analysis for NK and T cell-associated markers was performed at day 23.

Generation of CD56+ cells from RAG1+ cells

RAG1:GFP+ hematopoietic cells were sorted using an Influx FACS sorter (BD) on day 19 of PSC differentiation. 5000 sorted RAG1+ cells were plated per well of 96-well round bottom plates, which enabled cells to be positioned in the centre of wells to visualise RAG1:GFP fluorescence. Cells were cultured with IL7 20 ng/ml, IL15 20 ng/ml, or IL7 and IL15 both 20 ng/ml. The medium was carefully changed 2 days after replating (as day 2) and flow cytometry characterization was performed on day 4 after replating. Fluorescence images were taken using a Zeiss Observer Z1 fluorescent microscope and processed using Fiji for Mac OS X.

Erythroid and myeloid differentiation from day 12 cultures

To generate cells representing the erythroid and myeloid lineages, day 12 cultures were supplemented with either 2 units/ml EPO or 50 ng/ml MCSF (Peprotech), respectively. Fourteen days following the addition of EPO, non-adherent cells were analysed for expression of CD235a (Glycophorin A) and CD14 by flow cytometry and via bright field microscopy. For cultures undergoing myeloid differentiation, non-adherent cells were analysed between 1 week and 5 weeks following the addition of MCSF using either flow cytometry (CD14) or by performing cytospin analyses as described previously in ref. 72.

T Cell differentiation experiments

T cell differentiations were performed using multiple formats and different stromal cell lines expressing NOTCH ligands. For OP9 DLL4 Monolayer differentiations, one day prior to initiation of T-cell cultures, a tissue-culture treated 12-well plate was plated with $3\text{--}5 \times 10^4$ OP9 cells per well in α -MEM with 10% FCS, 1 \times GlutaMAX and 1 \times penicillin/streptomycin. Half an hour prior to the start of culture, wells were washed with PBS and media changed to RPMI 1640 with 4% B27, 30 μ M L-ascorbic acid 2-phosphate sesquimagnesium salt hydrate, 1 \times GlutaMAX and 1 \times penicillin/streptomycin with added cytokines (henceforth RB27) as detailed in the table below. Initiation of culture was performed by adding 10^5 days 12 CD45+ CD34+ blood progenitor cells per well to give a total volume of 1 ml of RB27 per well. Media top-up was performed after 3–4 days by adding another 1 ml of RB27. After one week, cells were passaged onto a fresh layer of OP9 cells as described before. Cell passage was performed by harvesting and mechanically dissociating the whole cells within each well and passing the cell mixture through a 40 μ m membrane to exclude cell clumps. The flowthrough fraction was collected by centrifugation and resuspended in 1 ml of fresh RB27. On weeks 1 and 2, DLL4hi cells were used, and for subsequent weeks, OP9 cells expressing an approximately 10-fold lower level of DLL4 were used (DLL4lo). One well was harvested weekly for flow cytometry analysis.

For MS5 DLL4 Monolayer differentiations, one day prior to initiation of T-cell culture, a tissue-culture treated 12-well plate was seeded with 5×10^4 MS5 cells expressing high levels of human DLL4 (a gift from Dr. Kirsten Canté-Barrett and Prof. Frank Staal, the Leiden University Medical Centre, Leiden, The Netherlands, henceforth referred to as MS5-hDLL4) per well in α -MEM with 10% FCS, 1 \times GlutaMAX and 1 \times penicillin/streptomycin. Half an hour prior to the start of culture, wells were gently washed with PBS and media changed to RPMI 1640 with 4% B27, 30 μ M L-ascorbic acid 2-phosphate

sesquimagnesium salt hydrate, 1 \times GlutaMAX and 1 \times penicillin/streptomycin with added cytokines (henceforth RB27). Initiation of culture was performed by adding 10^5 day 12 CD45+ CD34+ blood progenitor cells per well to produce a total volume of 1 ml of RB27 per well. Media top-up was performed in 3–4 days by adding another 1 ml of RB27. After a week, an 80% media change was performed by aspirating and replacing 80% of the media from each well with fresh RB27. One well was harvested weekly for flow cytometry analysis. A summary of the cytokines added is given in the table below. In this method, the following sequence of cytokine treatments was applied: Week 1 (5 ng/ml IL-7, 10 ng/ml FLT3L, 10 ng/ml SCF, and 20 ng/ml bFGF), week 2 (2 ng/ml IL-7, 10 ng/ml FLT3L, and 20 ng/ml bFGF), week 3 (1 ng/ml IL-7, 10 ng/ml FLT3L, and 20 ng/ml bFGF). Catalogue numbers and suppliers for cytokines were as described above).

In addition to the monolayer differentiation format described above, the same MS5 cells expressing DLL4 described above were used to generate ATOs⁹ Half an hour prior to the start of the experiment, a 40 μ m Millicell 6-well transwell insert (EMD Millipore, Billerica, MA; Cat. PICMORG50) was placed on top of 1 mL of T-cell media with cytokines to create an air–liquid interface (cytokines summarised in table below). Each ATO was formed by mixing 1.5×10^5 MS5-hDLL4 cells and 10^4 -day 15 CD45+ CD34+ blood progenitor cells. The cell mixture was concentrated by centrifugation and the cells were resuspended in a 5 μ l medium to create a slurry that was then plated at the air–liquid interface. Each transwell insert was plated with a maximum of 5 ATOs. Media change was performed every two days with fresh T-cell media for the first two weeks, followed by RB27 for the remainder of the differentiation. ATOs were harvested every week for FACS analysis. In this method, the following sequence of cytokine treatments was applied: Week 1 (5 ng/ml IL-7, 10 ng/ml FLT3L, 10 ng/ml SCF, and 20 ng/ml bFGF), week 2 (2 ng/ml IL-7, 10 ng/ml FLT3L, and 20 ng/ml bFGF), week 3 (1 ng/ml IL-7, 10 ng/ml FLT3L, and 20 ng/ml bFGF). Catalogue numbers and suppliers for cytokines were as described above).

In a further iteration of T cell differentiation experiments relevant to Supplementary Fig. 2c, we constructed ATO cultures as described by Seet et al. ref. 24. The MS5-DLL4 expressing cells used for this experiment were received as a gift from the Crooks laboratory at the University of California, Los Angeles. Half an hour prior to the start of the experiment, a 40 μ m Millicell 6-well transwell insert (EMD Millipore, Billerica, MA; Cat. PICMORG50) was placed on top of 1 ml of T-cell media with 5 ng/ml SCF, 5 ng/ml IL7, 5 ng/ml FLT3L, and 20 ng/ml bFGF to create an air–liquid interface. Each ATO was formed by mixing 1.5×10^5 MS5-hDLL4 cells and 10^4 days 23 CD45+ CD34+ CD7+ T-lineage progenitor cells. The cell mixture was spun down and made into a 5 μ l cell slurry that was then plated at the air–liquid interface. Each transwell insert was plated with a maximum of five ATOs. Media change was performed every two days with fresh T-cell media for five weeks. ATOs were harvested every week for FACS analysis. At week 5 of culture, ATO-derived TCR+ cells were assessed for the expression of CD45RA, CCR7, and L-selectin.

For proliferation assays, multiple D35 ATOs were pooled and sorted to obtain TCR $\alpha\beta$ + CD8 + SP T-cells. Sorted CD8 SP T-cells were stained with CellTrace Violet (Invitrogen), following the manufacturer's instructions. Stained T-cells were then plated onto a U-bottom 96-well plate pre-coated overnight with 5 μ g/ml anti-CD3 (BD Pharmingen, clone OKT3) and 1 μ g/ml anti-CD28 (BD Pharmingen, clone NA/LE) in the presence of 100 IU/ml recombinant human IL-2 (Peprotech). All cells were maintained in T-cell media without FCS. Cells were harvested after four days and seven days of culture. On day four, a half-media change was performed.

B cell differentiation experiments

RM-RAG1:GFP iPSCs³⁶ were used to assess the B lineage differentiation potential of blood cell progenitors generated at differentiation day 12. Briefly, B cell differentiations using the non-adherent cell fraction from

day 12 cultures were seeded onto a monolayer of MS5 stromal cells in RB27 medium (as detailed above) supplemented with IL7, 1 ng/ml, SCF 5 ng/ml, FGF2, 5 ng/ml; IL3 5 ng/ml, with medium changed every 3–4 days. Cultures were examined for the generation of B cell progenitors using flow cytometry analysis for expression of CD19 in conjunction with RAG1 (GFP).

Endothelial tube assays

To examine the tube-forming ability of cells generated during differentiation, cryopreserved differentiation day 6 RM-tTom⁷³ endothelial cells were thawed into T cell medium (supplemented with day 6 growth factors) and seeded onto adherent tissue culture plates to enable recovery. The following day, cells were detached from the plates using TrypLE™ Select (ThermoFisher), counted, and then 150,000 cells were resuspended in T cell media containing VEGF 50 ng/ml, EGF 10 ng/ml, FGF2 10 ng/ml, hydrocortisone at 10 ng/ml, as described previously⁷⁴. Resuspended cells were then gently layered over a film of Matrigel (Merk) (300 µl/each well of a 24-well plate) and incubated for 24 h. Cultures were imaged using an LSM900 confocal microscope and analysed using ImageJ.

Flow cytometry and cell sorting

Anti-human conjugated antibodies used for flow cytometry are as follows. Antibody-fluorochrome (supplier, catalogue number, clone number, dilution used): CD3-APC (BioLegend, 300412, clone number UCHT1, dilution 1:10), CD4-PE (BioLegend, 300508, RPA-T4, 1:30), CD4-BV510 (BioLegend, 357419, A161A1, 1:50), CD7-APC (BD Pharmingen, 561604, MT-701, 1:50), CD8α-PE-Cy7 (BioLegend, 344712, SK1), CD8α-PE/Fire700 (BioLegend, 344765, SK1, 1:50), CD13-PE-Cy7 (BioLegend, 301712, WM15, 1:100), CD14-PE-Cy7 (BioLegend, 301814, MSE2, 1:100), CD16-APC-Cy7 (BD Pharmingen, 557758, 3G8, 1:20), CD16-PE-Cy7 (BioLegend, 302016, 3G8, 1:40), CD19-BV421 (BD Pharmingen, 302234, HIB19, 1:20), CD34-BV421 (BioLegend, 343610, 581, 1:50), CD34-PE-Cy7 (BioLegend, 343516, 581, 1:100), CD43-PE (BioLegend, 343204, 10G7, 1:50), CD45-BV421 (BioLegend, 304032, HI30, 1:30), CD45RA-BV421 (BioLegend, 304129, HI00, 1:50), CD56-PE (BD Pharmingen, 555516, B159, 1:50), CD94-BV605 (BD Bioscience, 743950, HP-3D9, 1:50), CD127/IL7R-PE (BioLegend, 351304, AO19D5, 1:50), CD159a-BV605 (BD Bioscience, 747921, 131411, 1:50), CD159c-BV605 (BD Bioscience, 748166, 134591, 1:50), CD161-PE-Vio770 (MACS, 130-113-594, 191B8, 1:50), CD235a-PE (BD Pharmingen, 555570, GA-R2 (HIR2), 1:2000), CD314-BV605 (BD Bioscience, 743130, U21-1283, 1:50), CDH5/V-Cadherin-FITC (BD Pharmingen, 560411, 55-7H1, 1:20), CCR7-PE-Cy7 (BioLegend, 353225, G043H7, 1:50), CXCR4-PE (BioLegend, 306506, 12G5, 1:50), DLL4-APC (BioLegend, 346508, MHD4-46, 1:40), JAG1-APC (BioLegend, 399105, W16199B, 1:30), KDR-AF647 (BioLegend, 359910, 7D4-6, 1:50), L-Selectin-APC (BioLegend, 304809, DREG-56, 1:50), NKp08-PE (BioLegend, 346706, 5D12, 1:50), TCRα/b-APC (BioLegend, 306728, IP26, 1:20).

Conjugated antibodies were diluted in FACS wash buffer (PBS supplemented with 2–5% foetal bovine serum) and incubated with cells for 20 min on ice. The cell suspension was washed twice with FACS wash solution to remove unbound antibodies and resuspended in FACS wash solution containing 1 µg/ml propidium iodide. Cell surface staining was examined by Becton Dickinson (BD) LSRFortessa Cell Analyser. Flow cytometry data was analyzed using the FlowLogic program (7.2.1, Data-Nova). Alternatively, cell purification was performed using a BD FACSaria FUSION or Influx cell sorter based on cell surface staining or the expression of a fluorescent reporter. Cells were collected using a 5 ml FACS tube containing 0.5 ml cold foetal calf serum.

Immunofluorescence and antibodies

Differentiated cells were fixed with 4% paraformaldehyde solution for 5 min at room temperature. Cells were blocked in a blocking buffer (PBS + 10% FCS + 0.1% Triton-X) for 1 h at room temperature. Primary

antibodies were diluted in blocking buffer and incubated overnight at 4 °C. Cells were washed three times with PBS, then stained with secondary antibodies diluted in blocking buffer for 1 h at room temperature. Stained cells were imaged using a Zeiss confocal LSM 780 inverted microscope. Image analysis was performed using ImageJ software. Antibodies: Mouse Anti-Human DLK1, Abcam, ab119930, 1:200, AB_10902607; Alexa Fluor 647 Mouse Anti-Human CD144, BD Biosciences, 561567, 1:50, AB_10712766; Alexa Fluor 647 Mouse IgG1k Isotype Control, BD Biosciences, 565571, 1:50, AB_2687590; Donkey Anti-Mouse IgG (H + L) Highly-Cross Adsorbed Secondary Antibody, Alexa Fluor 594, Thermo-Fisher, A21203, 1:1500, AB_141633

51Chromium release assay

K562 target cells were labelled with 100 µCi Chromium-51 (51Cr, PerkinElmer) for 1 h at 37 °C and subsequently co-cultured with PSC-derived NK cells or NK cells freshly isolated from healthy donors' peripheral blood mononuclear cells (PBMC) by NK Cell Isolation Kit (Miltenyi Biotec). NK cells were added in triplicate wells at effector: target ratios from 4:1 to 1:1. Wells with target cells alone (spontaneous release) and target cells with 10% Triton X 100 (maximum release) were included as controls. After 4-h or 16-h co-culture, cells were spun down and supernatants were collected. The amount of 51Cr released in the supernatants was detected using a gamma counter (Wallac Wizard 1470). The %specific lysis was calculated by [(experimental release – spontaneous release)/(maximum release – spontaneous release)] × 100.

K562 killing assay using flow cytometry

K562 cells were maintained in RPMI + 10% FCS + 1% Pen Strep (medium changed weekly). For killing experiments, cells were passaged the day before and then given fresh medium on the morning of the experiment. Approximately 1 million K562 target cells suspended in 1 ml of PBS were labelled with 1 µM carboxyfluorescein succinimidyl ester for 10 min at 37°, in the dark. Cells were pelleted and resuspended in 1 ml of PBS + 10% Foetal calf serum—and incubated for a further 30 mins at 37°. Cells were then concentrated by centrifugation, washed twice with PBS 4 °C and then resuspended in day 19 medium (including growth factors) at 1–3 million cells per ml. Flow cytometry K562 killing assays were performed essentially as described by ref. 75. Labelled K562 cells distributed into each well of a round-bottomed 96 well tray at between 25,000–150,000 cells per well—with each well in any given experiment receiving the same number of K562 cells. Non-adherent (NK-effector) cells from day 28–32 cultures that had been grown in medium supplemented with IL15 from day 15 were added to each well to give effector: target (K562) cell ratios as indicated. Following 4 h of incubation at 37 °C, counting beads were added to each well in a medium containing 1 µg/ml (check) DAPI. Flow cytometry was used to assess the number of viable (DAPI negative, CSFE+ cells). The flow cytometer was programmed to acquire a set volume uniformly for each separate experimental set-up. Counting beads were used as an independent measure of consistency. The number of viable K562 cells per given volume/bead count was used to calculate the overall K562 viability for each sample. Percentage viability was calculated as the fraction of viable K562 cells in the test well relative to the number of viable K562 cells present in the corresponding control wells (or the average of control wells) × 100. Each assay for a given effector/target ratio was performed at least in triplicate.

Single-cell RNA sequencing and bioinformatics

Single-cell suspension samples were prepared at 1,000,000 cells/ml with at least 90% cell viability. The Victorian Clinical Genetics Service performed the library preparation and sequencing following the 10× Genomics Cell Preparation Guide (www.10xgenomics.com). Sequencing was performed with the Illumina Novaseq-6000 system for a target of 300 million reads per sample with 6000 cells and 50,000 read depth.

Fastq files generated from the Illumina sequencing were mapped against the human reference genome GRCh38-1.2.0 with CellRanger software using the count function [2]. An additional CellRanger aggregation with the aggr function was applied to group all samples into one output 'filtered_gene-bc_matrices' folder. The R platform along with its suite of single-cell bioinformatic packages with R version 4.2.1 was used for single-cell data analysis (www.R-project.org). Seurat (v4.1.1) was used for single-cell data pre-processing and subsequent downstream analysis and visualizations. Cells that were not within the quality control boundaries (see GitHub) were excluded. The standard Seurat pipeline includes log normalization at a scale factor of 10,000, scale data to centre gene expression values and principal component analysis to reduce dimensions. The FindCluster function was used to identify clusters within each sample.

PSC-derived cells were integrated with foetal human embryonic AGM and foetal liver data at developmental stages week 4.5–15¹⁹). The integration was performed with Seurat's FindIntegrationAnchors and IntegrateData function based on a list of genes identified by the SelectIntegrationFeatures function. The human embryonic data, as a reference along with canonical markers was used for the identification of cell identities of each cluster. The FindAllMarkers function was used to produce a list of genes that were specific to each cluster which were then used in visualization plots such as heatmaps, violin plots, dot plots and feature plots. Differential gene per cluster was performed with the FindMarkers function.

Downstream analysis including machine learning-based analysis and neural networks to predict PSC cluster identities was completed with ACTINN version 2⁴¹ (see GitHub to access the test and reference datasets used). Gene ontology was completed with Metascape⁷⁶ and inputting the gene list identified by the FindAllMarkers function. CellChat version 1.4.0⁴² was used for the ligand and receptor pair analysis following the standard CellChat vignette. Pseudotime analysis to track the hematopoiesis and lymphopoiesis within our cultures utilized the SeuratWrappers package version 0.3.0, as well as following the Monocle3 vignette⁷⁷ to select the root starting cells as the "HE (hemogenic endothelial cell)" cluster.

Analysis of endothelial to hematopoietic transition in Fig. 2e utilizes PSC-derived cells from days 12 and 15 based on expression of *CD31* or *CD34* and *RUNX1* or *CDH5*. The analysis of blood cells from HSPC to lymphoid cells utilizes a subset of PSC-derived cells based on the "HSPC", "ILC" and "RAG + Lymph" clusters identified in Fig. 2a. To investigate the heterogeneity and different ILC clusters in Fig. 3e, cells from "ILC" and "ILC_cyc" clusters were pooled from the Fig. 3a. Additionally cell cycling genes were regressed out to avoid influence by ILC cells' cycling state. Genes displayed in Supplementary Fig. 4 heatmap were the specific genes of each cluster based on reclustered and pooled cells identified as the "HSPC", Lymph_pro1, pro2 and pro3 clusters in Fig. 3a. Cells in Supplementary Fig. 4d were based on pooling of *RAG1*⁺ cells from day 19 and 25 samples. The average expression function was used to calculate the mean of *RAG1* average expression across all clusters. Cells that were above the mean average expression of 2.259 (4sf) were labelled as "RAG-high" and those lower "RAG-low". All subsets described above were re-clustered with the standard Seurat pipeline.

Statistics

Statistical analysis was performed in Prism (GraphPad, Version 8.0.2) by *t*-test, one-way ANOVA or two-way ANOVA tests as indicated in figure legends.

Reporting summary

Further information on research design is available in the Nature Portfolio Reporting Summary linked to this article.

Data availability

RNA sequencing raw data is available in the public GEO data repository with access code [GSE217705](https://www.ncbi.nlm.nih.gov/geo/query/acc.cgi?acc=GSE217705). Seurat data objects and codes are available at GitHub: <https://github.com/jackyyishengli/Sun-and-Motazedian-et-al-2023>. Source data are provided in this paper.

References

1. Sasaki, K. & Matsumura, G. Haemopoietic cells of yolk sac and liver in the mouse embryo: a light and electron microscopical study. *J. Anat.* **148**, 87–97 (1986).
2. Palis, J., McGrath, K. E. & Kingsley, P. D. Initiation of hematopoiesis and vasculogenesis in murine yolk sac explants. *Blood* **86**, 156–163 (1995).
3. Hamaguchi, I. et al. In vitro hematopoietic and endothelial cell development from cells expressing TEK receptor in murine aorta–gonad–mesonephros region. *Blood* **93**, 1549–1556 (1999).
4. Medvinsky, A. & Dzierzak, E. Definitive hematopoiesis is autonomously initiated by the AGM region. *Cell* **86**, 897–906 (1996).
5. de Bruijn, M. F., Speck, N. A., Peeters, M. C. & Dzierzak, E. Definitive hematopoietic stem cells first develop within the major arterial regions of the mouse embryo. *EMBO J.* **19**, 2465–2474 (2000).
6. Sanchez, M. J., Holmes, A., Miles, C. & Dzierzak, E. Characterization of the first definitive hematopoietic stem cells in the AGM and liver of the mouse embryo. *Immunity* **5**, 513–525 (1996).
7. Cumano, A., Ferraz, J. C., Klaine, M., Di Santo, J. P. & Godin, I. Intraembryonic, but not yolk sac hematopoietic precursors, isolated before circulation, provide long-term multilineage reconstitution. *Immunity* **15**, 477–485 (2001).
8. Cumano, A., Dieterlen-Lievre, F. & Godin, I. Lymphoid potential, probed before circulation in mouse, is restricted to caudal intraembryonic splanchnopleura. *Cell* **86**, 907–916 (1996).
9. Li, L., Leid, M. & Rothenberg, E. V. An early T cell lineage commitment checkpoint dependent on the transcription factor Bcl11b. *Science* **329**, 89–93 (2010).
10. Medetgul-Ernar, K. & Davis, M. M. Standing on the shoulders of mice. *Immunity* **55**, 1343–1353 (2022).
11. Sun, S. et al. CD90 marks a mesenchymal program in human thymic epithelial cells in vitro and in vivo. *Front. Immunol.* **13**, 846281 (2022).
12. Ivanovs, A. et al. Human haematopoietic stem cell development: from the embryo to the dish. *Development* **144**, 2323–2337 (2017).
13. Ditadi, A., Sturgeon, C. M. & Keller, G. A view of human haematopoietic development from the petri dish. *Nat. Rev. Mol. Cell Biol.* **18**, 56–67 (2017).
14. Fidanza, A. et al. Single cell analyses and machine learning define hematopoietic progenitor and HSC-like cells derived from human PSCs. *Blood* <https://doi.org/10.1182/blood.2020006229> (2019).
15. Sturgeon, C. M., Ditadi, A., Awong, G., Kennedy, M. & Keller, G. Wnt signaling controls the specification of definitive and primitive hematopoiesis from human pluripotent stem cells. *Nat. Biotechnol.* **32**, 554–561 (2014).
16. Ditadi, A. et al. Human definitive haemogenic endothelium and arterial vascular endothelium represent distinct lineages. *Nat. Cell Biol.* **17**, 580–591 (2015).
17. Uenishi, G. I. et al. NOTCH signaling specifies arterial-type definitive hemogenic endothelium from human pluripotent stem cells. *Nat. Commun.* **9**, 1828 (2018).
18. Ng, E. S. et al. Differentiation of human embryonic stem cells to HOXA⁺ hemogenic vasculature that resembles the aorta–gonad–mesonephros. *Nat. Biotechnol.* **34**, 1168–1179 (2016).
19. Calvanese, V. et al. Mapping human haematopoietic stem cells from haemogenic endothelium to birth. *Nature* **604**, 534–540 (2022).

20. Zeng, Y. et al. Tracing the first hematopoietic stem cell generation in human embryo by single-cell RNA sequencing. *Cell Res.* **29**, 881–894 (2019).
21. Iriguchi, S. et al. A clinically applicable and scalable method to regenerate T-cells from iPSCs for off-the-shelf T-cell immunotherapy. *Nat. Commun.* **12**, 430 (2021).
22. Shukla, S. et al. Progenitor T-cell differentiation from hematopoietic stem cells using Delta-like-4 and VCAM-1. *Nat. Methods* **14**, 531–538 (2017).
23. Jing, R. et al. EZH1 repression generates mature iPSC-derived CAR T cells with enhanced antitumor activity. *Cell Stem Cell* **29**, 1181–1196.e1186 (2022).
24. Seet, C. S. et al. Generation of mature T cells from human hematopoietic stem and progenitor cells in artificial thymic organoids. *Nat. Methods* **14**, 521–530 (2017).
25. Montel-Hagen, A. et al. Organoid-induced differentiation of conventional T cells from human pluripotent stem cells. *Cell Stem Cell* **24**, 376–389.e378 (2019).
26. Schmitt, T. M. & Zúñiga-Pflücker, J. C. Induction of T cell development from hematopoietic progenitor cells by delta-like-1 in vitro. *Immunity* **17**, 749–756 (2002).
27. Van de Walle, I. et al. Jagged2 acts as a delta-like notch ligand during early hematopoietic cell fate decisions. *Blood* **117**, 4449–4459 (2011).
28. Sun, S. et al. Lymphoid cell development from fetal hematopoietic progenitors and human pluripotent stem cells. *Immunol. Rev.* **315**, 154–170 (2023).
29. Hermanson, D. L. et al. Induced pluripotent stem cell-derived natural killer cells for treatment of ovarian cancer. *Stem Cells* **34**, 93–101 (2016).
30. Knorr, D. A. et al. Clinical-scale derivation of natural killer cells from human pluripotent stem cells for cancer therapy. *Stem Cells Transl. Med.* **2**, 274–283 (2013).
31. Dege, C. et al. Potently cytotoxic natural killer cells initially emerge from erythro-myeloid progenitors during mammalian development. *Dev. Cell* **53**, 229–239.e7 (2020).
32. Ng, E. S., Davis, R. P., Azzola, L., Stanley, E. G. & Elefanty, A. G. Forced aggregation of defined numbers of human embryonic stem cells into embryoid bodies fosters robust, reproducible hematopoietic differentiation. *Blood* **106**, 1601–1603 (2005).
33. Grzywacz, B. et al. Natural killer-cell differentiation by myeloid progenitors. *Blood* **117**, 3548–3558 (2011).
34. Chen, Q. et al. Delineation of natural killer cell differentiation from myeloid progenitors in human. *Sci. Rep.* **5**, 15118 (2015).
35. Liu, C. et al. Delineating spatiotemporal and hierarchical development of human fetal innate lymphoid cells. *Cell Res.* **31**, 1106–1122 (2021).
36. Motazedian, A. et al. Multipotent RAG1+ progenitors emerge directly from haemogenic endothelium in human pluripotent stem cell-derived haematopoietic organoids. *Nat. Cell Biol.* **22**, 60–73 (2020).
37. Loh, K. M. et al. Mapping the pairwise choices leading from pluripotency to human bone, heart, and other mesoderm cell types. *Cell* **166**, 451–467 (2016).
38. Davis, R. P. et al. Targeting a GFP reporter gene to the MIXL1 locus of human embryonic stem cells identifies human primitive streak-like cells and enables isolation of primitive hematopoietic precursors. *Blood* **111**, 1876–1884 (2008).
39. Itoh, K. et al. Reproducible establishment of hemopoietic supportive stromal cell lines from murine bone marrow. *Exp. Hematol.* **17**, 145–153 (1989).
40. Mohtashami, M., Shah, D. K., Kianizad, K., Awong, G. & Zúñiga-Pflücker, J. C. Induction of T-cell development by delta-like 4-expressing fibroblasts. *Int. Immunol.* **25**, 601–611 (2013).
41. Ma, F. & Pellegrini, M. ACTINN: automated identification of cell types in single cell RNA sequencing. *Bioinformatics* **36**, 533–538 (2020).
42. Jin, S. et al. Inference and analysis of cell-cell communication using CellChat. *Nat. Commun.* **12**, 1088 (2021).
43. Popescu, D. M. et al. Decoding human fetal liver haematopoiesis. *Nature* **574**, 365–371 (2019).
44. Huntington, N. D. et al. IL-15 trans-presentation promotes human NK cell development and differentiation in vivo. *J. Exp. Med.* **206**, 25–34 (2009).
45. Carrette, F. & Surh, C. D. IL-7 signaling and CD127 receptor regulation in the control of T cell homeostasis. *Semin. Immunol.* **24**, 209–217 (2012).
46. Vranjkovic, A., Crawley, A. M., Gee, K., Kumar, A. & Angel, J. B. IL-7 decreases IL-7 receptor alpha (CD127) expression and induces the shedding of CD127 by human CD8+ T cells. *Int. Immunol.* **19**, 1329–1339 (2007).
47. Park, J. E. et al. A cell atlas of human thymic development defines T cell repertoire formation. *Science* **367**, eaay3224 (2020).
48. Koga, S. et al. Peripheral PDGFRalpha(+)gp38(+) mesenchymal cells support the differentiation of fetal liver-derived ILC2. *J. Exp. Med.* **215**, 1609–1626 (2018).
49. Karo, J. M., Schatz, D. G. & Sun, J. C. The RAG recombinase dictates functional heterogeneity and cellular fitness in natural killer cells. *Cell* **159**, 94–107 (2014).
50. Kim, J. et al. A flow cytometry-based whole blood natural killer cell cytotoxicity assay using overnight cytokine activation. *Front. Immunol.* **11**, 1851 (2020).
51. Wagner, J. et al. A two-phase expansion protocol combining interleukin (IL)-15 and IL-21 improves natural killer cell proliferation and cytotoxicity against rhabdomyosarcoma. *Front. Immunol.* **8**, 676 (2017).
52. Yang, D. et al. Modeling human multi-lineage heart field development with pluripotent stem cells. *Cell Stem Cell* **29**, 1382–1401.e1388 (2022).
53. Veres, A. et al. Charting cellular identity during human in vitro beta-cell differentiation. *Nature* **569**, 368–373 (2019).
54. Kanton, S. et al. Organoid single-cell genomic atlas uncovers human-specific features of brain development. *Nature* **574**, 418–422 (2019).
55. Luff, S. A. et al. Identification of a retinoic acid-dependent haemogenic endothelial progenitor from human pluripotent stem cells. *Nat. Cell Biol.* **24**, 616–624 (2022).
56. Yokomizo, T. et al. Independent origins of fetal liver haematopoietic stem and progenitor cells. *Nature* **609**, 779–784 (2022).
57. Calvanese, V. et al. MLLT3 governs human haematopoietic stem-cell self-renewal and engraftment. *Nature* **576**, 281–286 (2019).
58. Patel, S. H. et al. Lifelong multilineage contribution by embryonic-born blood progenitors. *Nature* **606**, 747–753 (2022).
59. Dignum, T. et al. Multipotent progenitors and hematopoietic stem cells arise independently from hemogenic endothelium in the mouse embryo. *Cell Rep.* **36**, 109675 (2021).
60. Tian, Y. et al. The first wave of T lymphopoiesis in zebrafish arises from aorta endothelium independent of hematopoietic stem cells. *J. Exp. Med.* **214**, 3347–3360 (2017).
61. Winer, H. et al. IL-7: comprehensive review. *Cytokine* **160**, 156049 (2022).
62. Andreu-Ballester, J. C. et al. Deficit of interleukin-7 in serum of patients with Crohn's disease. *Inflamm. Bowel Dis.* **19**, E30–E31 (2013).
63. Park, L. S. et al. Cloning of the murine thymic stromal lymphopoietin (TSLP) receptor: Formation of a functional heteromeric complex requires interleukin 7 receptor. *J. Exp. Med.* **192**, 659–670 (2000).
64. Regev, A. et al. The human cell atlas. *Elife* **6**, e27041 (2017).

65. Bassing, C. H., Swat, W. & Alt, F. W. The mechanism and regulation of chromosomal V(D)J recombination. *Cell* **109**, S45–S55 (2002).
66. Pilbeam, K. et al. The ontogeny and fate of NK cells marked by permanent DNA rearrangements. *J. Immunol.* **180**, 1432–1441 (2008).
67. Dobbs, K. et al. Natural killer cells from patients with recombinase-activating gene and non-homologous end joining gene defects comprise a higher frequency of CD56(bright) NKG2A(+++) Cells, and yet display increased degranulation and higher perforin content. *Front. Immunol.* **8**, 798 (2017).
68. Thomson, J. A. et al. Embryonic stem cell lines derived from human blastocysts. *Science* **282**, 1145–1147 (1998).
69. Vlahos, K. et al. Generation of iPSC lines from peripheral blood mononuclear cells from 5 healthy adults. *Stem Cell Res.* **34**, 101380 (2019).
70. Chen, G. et al. Chemically defined conditions for human iPSC derivation and culture. *Nat. Methods* **8**, 424–429 (2011).
71. Costa, M., Sourris, K., Hatzistavrou, T., Elefanty, A. G. & Stanley, E. G. Expansion of human embryonic stem cells in vitro. *Curr. Protoc. Stem Cell Biol.* **1**, Unit 1C.1.1–1C.1.7 (2008).
72. Sun, S. et al. Human pluripotent stem cell-derived macrophages host *Mycobacterium abscessus* infection. *Stem Cell Rep.* **17**, 2156–2166 (2022).
73. Kao, T. et al. GAPTrap: a simple expression system for pluripotent stem cells and their derivatives. *Stem Cell Rep.* **7**, 518–526 (2016).
74. Bruveris, F. F. et al. Human yolk sac-like haematopoiesis generates RUNX1-, GFI1- and/or GFI1B-dependent blood and SOX17-positive endothelium. *Development* **147**, 15 (2020).
75. Kandarian, F., Sunga, G. M., Arango-Saenz, D., Rossetti, M. A flow cytometry-based cytotoxicity assay for the assessment of human NK cell activity. *J. Vis. Exp.* **9**, 56191 (2017).
76. Zhou, Y. et al. Metascape provides a biologist-oriented resource for the analysis of systems-level datasets. *Nat. Commun.* **10**, 1523 (2019).
77. Cao, J. et al. The single-cell transcriptional landscape of mammalian organogenesis. *Nature* **566**, 496–502 (2019).

Acknowledgements

The authors acknowledge Tanya Labonne and Xavier Busuttil-Crellin for technical assistance, and Matt Burton and Eleanor Jones for flow cytometry assistance. We acknowledge funding by the NHMRC through fellowships GNT1117596 (A.G.E) and GNT1079004 (E.G.S.) and research grants GNT1068866, GNT1129861 (A.G.E. and E.G.S.), GNT1164577, GNT2012936 (E.S.N.), GNT2012535 (A.G.E) and GNT1186019 (E.G.S.). This work was supported by the Australian Research Council Special Research Initiative in Stem Cells (Stem Cells Australia) and by the Stafford Fox Medical Research Foundation. This study was supported by the Novo Nordisk Foundation Centre for Stem Cell Medicine, funded by Novo Nordisk Foundation grant NNF21CC0073729 (A.G.E, E.G.S, and E.S.N). The work was also supported by China Postdoctoral Science Foundation grant YJ20220249 (S.S.). Additional infrastructure funding for the Murdoch Children's Research Institute was provided by the Australian Government National Health and Medical Research Council

Independent Research Institute Infrastructure Support Scheme and the Victorian Government's Operational Infrastructure Support Program.

Author contributions

Conceptualization: S.S., A.M., and E.G.S. Methodology: S.S., A.M., J.Y.L., and E.G.S. Investigation and data collection: S.S., A.M., K.W., J.J.Z., P.J.N., K.A.S., L.R.N., A.S., K.T., J.V.S., and Y.Y. Bioinformatics analysis: J.Y.L. and S.S. Data interpretation: S.S. and E.G.S. Manuscript preparation: S.S. Supervision and manuscript editing: E.G.S., A.G.E., and E.S.N. Funding acquisition: A.G.E., E.G.S., and E.S.N. All authors have read and approved the version for publication.

Competing interests

A Patent application, International (PCT) Patent No. PCT/AU2024/050206 (Inventors, S.S., A.M., E.G.S., E.S.N., A.G.E.), has been filed in relation to the methodology described in this manuscript. The remaining authors declare no competing interests.

Additional information

Supplementary information The online version contains supplementary material available at <https://doi.org/10.1038/s41467-024-51974-7>.

Correspondence and requests for materials should be addressed to Shicheng Sun or Edouard G. Stanley.

Peer review information *Nature Communications* thanks Ana Cumano, and the other, anonymous, reviewer(s) for their contribution to the peer review of this work. A peer review file is available.

Reprints and permissions information is available at <http://www.nature.com/reprints>

Publisher's note Springer Nature remains neutral with regard to jurisdictional claims in published maps and institutional affiliations.

Open Access This article is licensed under a Creative Commons Attribution-NonCommercial-NoDerivatives 4.0 International License, which permits any non-commercial use, sharing, distribution and reproduction in any medium or format, as long as you give appropriate credit to the original author(s) and the source, provide a link to the Creative Commons licence, and indicate if you modified the licensed material. You do not have permission under this licence to share adapted material derived from this article or parts of it. The images or other third party material in this article are included in the article's Creative Commons licence, unless indicated otherwise in a credit line to the material. If material is not included in the article's Creative Commons licence and your intended use is not permitted by statutory regulation or exceeds the permitted use, you will need to obtain permission directly from the copyright holder. To view a copy of this licence, visit <http://creativecommons.org/licenses/by-nc-nd/4.0/>.

© The Author(s) 2024